



# Journal of Agrometeorology

ISSN : 0972-1665 (print), 2583-2980 (online)

Vol. No. 25 (2) : 262 - 267 (June- 2023)

DOI : <https://doi.org/10.54386/jam.v25i2.2155>

<https://journal.agrimetassociation.org/index.php/jam>



## Research Paper

### Spatial variations of LST and NDVI in Muzaffarpur district, Bihar using Google earth engine (GEE) during 1990-2020

BHARTENDU SAJAN<sup>1</sup>, SHRUTI KANGA<sup>2\*</sup>, SURAJ KUMAR SINGH<sup>3</sup>, VARUN NARAYAN MISHRA<sup>4</sup> and BOJAN DURIN<sup>5</sup>

<sup>1</sup>Centre for Climate Change and Water Research, Suresh Gyan Vihar University, Jaipur, Rajasthan 302017, India

<sup>2</sup>Department of Geography, School of Environment and Earth Sciences, Central University of Punjab, VPO-Ghudda, Bathinda 151401, Punjab, India,

<sup>3</sup>Centre for Sustainable Development, Suresh Gyan Vihar University, Jaipur 302017, Rajasthan, India

<sup>4</sup>Amity Institute of Geoinformatics & Remote Sensing (AIGIRS), Amity University, Sector 125, Noida 201313, Gautam Buddha Nagar, India,

<sup>5</sup>Department of Civil Engineering, University North, Varaždin 42000, Croatia.

Corresponding author's email: [shruti.kanga@cup.edu.in](mailto:shruti.kanga@cup.edu.in)

#### ABSTRACT

The aim of this study is to analyze land cover changes and their effects on land surface temperature (LST) and normalized difference vegetation index (NDVI) in Muzaffarpur district, Bihar, India. The research utilized Landsat 5 and 8 satellite images taken every five years from 1990 to 2020 to classify seven land cover types, namely built-up areas, wetlands, fallow lands, croplands, vegetation, and water bodies, using the Artificial Neural Network technique in ENVI 5.1. The resulting land cover maps reveal a significant decrease in cropland area during the studied period, while fallow land area decreased from 48.06% to 35.79%. Analysis of LST and NDVI data showed a strong negative correlation ( $R^2 < -0.0057$ ) for all years, except for a weak positive correlation ( $R^2 > 0.006$ ). NDVI values were highest in agricultural lands with the lowest LST values, while fallow land areas showed the opposite trend. The study suggests that vegetation and fallow land are crucial determinants of the spatial and temporal variations in NDVI and LST, relative to urban and water cover categories.

**Key words:** Land use land cover, Land surface temperature, NDVI, Correlation

Increasing population, economic development, and migration have changed cities' land use and land cover (LULC). Climate change, global warming, and local climate fluctuations changes the Earth's surface energy budget. Evaporation, solar radiation absorption, and biodiversity are affected by LULC distribution variations. Industrial and commercial areas are hotter than green places; hence urbanization enhances land surface temperatures. Biophysical variables modify land cover, whereas human activities change land use (Lambin *et al.*, 2001). Microclimates, biodiversity, ecosystem services, and environmental health are regulated by urban vegetation (Lin *et al.*, 2015). Vegetation cover decreases temperatures and improves urban ecology (Richards and Belcher 2019). Temperature is one of the important parameters affecting agriculture and hence, has widely been used in yield prediction incorporating spatial information (Bhagia *et al.*, 2005; Chaudhari

*et al.*, 2010; Dadhwal and Bhat, 2023). Urban land use change is complex and often transforms vast volumes of natural and semi-natural plants, lowering city greenery. Green regions protect biodiversity, biotic and abiotic ecosystems, and local, regional, and global land surface temperature (LST). Global warming is caused by damaging land use (Rakib *et al.*, 2020). Urban area management and sustainable city design require precise land use and cover data and urban surface thermal characteristics. Field research and manual data gathering to track these changes can be expensive, time-consuming, and inaccurate. Satellite imaging and remote sensing provide fast, accurate, and cost-effective data collecting and processing.

The Landsat series of satellites offers high-resolution estimations of land surface temperature (LST) that are particularly

**Article info - DOI:** <https://doi.org/10.54386/jam.v25i2.2155>

Received: 09 March 2023; Accepted: 21 April 2023; Published online : 25 May 2023

"This work is licensed under Creative Common Attribution-Non Commercial-ShareAlike 4.0 International (CC BY-NC-SA 4.0) © Author (s)"

beneficial for small-scale and local research. Although many LST algorithms have been proposed for Landsat, several of them necessitate calibration coefficients and input data that may not be easily accessible. While some datasets are available online, they can be unwieldy due to the large amounts of data that need to be managed. Google Earth Engine (GEE) can analyse huge data for remote sensing analysts. This paper aims to investigate the impact of land surface temperature (LST) on agriculture in Muzaffarpur district, Bihar using remote sensing and GIS tools. The study objectives include generating maps of LULC categories and NDVI, analyzing the temporal and spatial distribution of LST, and examining the correlation between LST and NDVI from 1990 to 2020. The research utilizes Google Earth Engine (GEE) and Landsat 5 and 8 data to accomplish these objectives.

## MATERIALS AND METHODS

### Study area

Muzaffarpur district is situated in northern Bihar, India, and covers an area of 3,175.9 square kilometers. It is located between 25° 53' N to 26° 25' N latitude and 84° 50' E to 85° 45' E longitude. The district serves as the headquarters of Tirhut Division, which was the ancient name for northern Bihar. The region is known for its fertile lands and is located in the Gangetic plain. Rivers such as Gandak, Budhi Gandak, Bagmati, and Lakhandei, as well as many streams, flow through the area. However, the region is also prone to floods (Fig.1).

This study employed Landsat satellite data for classifying land use/land cover (LULC) and measuring land surface temperature (LST) and NDVI over vast spatial scales. These specialized sensors can detect thermal infrared (TIR) radiation emitted by the land surface. The Landsat 5-TM data of May 11, 1990; Landsat 7-ETM+ data of May 5, 2000; Landsat 7-ETM+ data of May 26, 2010 and Landsat 8-OLI data of May 5, 2020 were used in the study.

### Image pre processing

In order to enable classification and eliminate systematic errors, the Landsat 4-5 TM images were subjected to atmospheric and radiometric corrections during the image pre-processing stage. However, no such corrections were required for Landsat 8 OLI/TIRS images. Image processing, analysis, and map production were carried out using ERDAS IMAGINE and ArcGIS software. To ensure seamless processing and classification, a mask of the area of interest (AOI) was generated from all images.

### LULC classification

ENVI 5.1 software was employed to classify images using an Artificial Neural Network (ANN) model. The images were classified based on various land use categories, such as built-up areas, vegetation, fallow land, cropland, litchi cultivation areas, wetlands, and water bodies.

### Accuracy assessment

The confusion matrix approach was used to evaluate the accuracy and effectiveness of the classified images, and metrics such

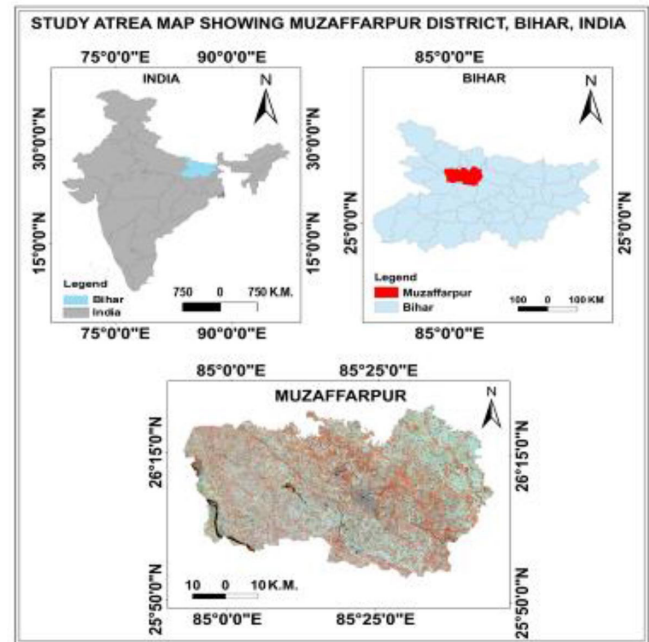


**Fig. 1:** Location map of Muzaffarpur district, Bihar

as kappa statistics, producer accuracy, user accuracy, and overall accuracy were calculated to provide a comprehensive understanding of the classification accuracy.

### Calculation of normalized difference vegetation index (NDVI)

The Google Earth Engine has a built-in function to compute NDVI from an image using the red and near infrared (NIR) frequency bands, which is then added as a new band. Since Landsat 5 and Landsat 8 have different band combinations for capturing the red and NIR band spectra, separate NDVI functions were utilized. Specifically, Landsat 5 uses band three for the red band and band four for the NIR band, while Landsat 8 uses band four for the red band and band five for the NIR band.

### Computation of land surface temperature (LST)

To maintain consistency with previous research and due to the simplicity of implementation, the single channel (SC) technique was utilized in this study to estimate land surface temperature (LST) from Landsat satellite data. This approach, which only requires one thermal infrared channel, has been widely used in previous studies by researchers such as (Dash *et al.*, 2002). Among the Landsat 5, 7, and 8 series, only Landsat 8 has two thermal bands, making the SC technique the best choice for this analysis. The LST (TS) was calculated using the radiative transfer equation and a SC technique by determining the radiance-at-the-sensor in a single band.

$$B(LST) = \frac{L_{sen} - L_{up} - \tau * (1 - \epsilon) * L_{down}/\pi}{\tau * \epsilon}$$

Where,  $\epsilon$  is the surface emissivity,  $\tau$  is the atmospheric transmissivity,  $B$  is the Planck function,  $L_{sen}$  is the radiance-at-the-sensor,  $L_{up}$  is the thermal path radiance,  $L_{down}$  is the down welling irradiance, and  $L_{up}$  is the thermal path radiance.

**Table 1:** Accuracy assessment of LULC maps of Muzaffarpur district

| Classes            | User's accuracy<br>(UA, %) | Producers' accuracy<br>(PA, %) |
|--------------------|----------------------------|--------------------------------|
| Built up area      | 90.3                       | 91.9                           |
| Wetland            | 95.4                       | 90.9                           |
| Fallow land        | 79.7                       | 86.0                           |
| Cropland           | 88.4                       | 90.9                           |
| Vegetation         | 79.7                       | 87.4                           |
| Litchi cultivation | 90.5                       | 86.8                           |
| Waterbody          | 97.4                       | 91.1                           |

### Thermal radiance-at-sensor from landsat

The Landsat level 1T products provided by USGS are available in GEE as an image collection, and the GEE function applies scaling factors to convert the digital numbers in the images to radiance-at-sensor values, ensuring a consistent 30m x 30m resolution for all products through a cubic convolution resampling technique.

### Brightness temperature and cloud mask

In this study, Landsat top-of-the-atmosphere (TOA) brightness temperature data were obtained from the GEE library's image collection. These data were generated by inverting the Planck function, and were accompanied by cloud cover data obtained using the Fmask technique, which can detect clouds, cloud shadows, and water surfaces in Landsat images (Zhu and Curtis 2012; Zhu *et al.*, 2015). The brightness temperature data were used to extract information about clouds, cloud shadows, and water surfaces.

### Surface reflectance

The Landsat surface reflectance, a high-level product developed by the Landsat Ecosystem Disturbance Adaptive Processing System (LEDAPS) (Masek *et al.*, 2017) provides surface reflectance data for six bands covering a wavelength range of 0.22-2.35µm and with a spatial resolution of 30m x 30m. In this study, the red and near-infrared bands are used to calculate NDVI, which is a prerequisite for computing the NDVI-based emissivity.

### Emissivity

The equation calculates the fraction of vegetation cover (FVC) based on NDVI thresholds for vegetated and non-vegetated surfaces and uses reference emissivities for these two surfaces to determine emissivity, resulting in a 30m x 30m spatial resolution NDVI-based emissivity product matching that of Landsat's thermal data.

$$FVC = \left[ \frac{NDVI - NDVI_{nonveg}}{NDVI_{veg} - NDVI_{nonveg}} \right]^2$$

$$\epsilon = \epsilon_{nonveg} \cdot (1 - FVC) + \epsilon_{veg} \cdot FVC$$

### Implementation of the LST algorithm in the GEE

The Landsat LST main module utilizes input information such as date range, Landsat satellite, region of interest, and NDVI-

based correction flag for emissivity to load collections of TOA brightness temperatures and surface reflectance, apply cloud masking, and use NDVI and FVC values to determine emissivity and apply the SC algorithm to Landsat TIR bands.

## RESULTS AND DISCUSSIONS

### LULC classification accuracy

In order to evaluate the effectiveness of the classification process, accuracy assessment is considered a critical aspect. The primary objective of this evaluation is to determine how effectively pixels were assigned to their respective land cover categories. During the accuracy assessment, areas that were easily identifiable on both Google Earth and Landsat images were given priority when selecting samples. The accuracy of the classification results is often determined using error matrix-based statistics, which include overall accuracy (OA), producer's accuracy (PA), and user's accuracy (UA). For this study, thematic maps for the years 1990, 2000, 2010, and 2020 were each subjected to an accuracy assessment. OA is calculated by dividing the number of correctly classified pixels by the total number of pixels, while PA is determined by dividing the number of correctly detected pixels by the total number of reference pixels. UA is calculated by dividing the number of correctly classified pixels for a particular class by the sum of the row totals. The classification accuracy of the LULC images is presented in Table 1.

### LULC changes

The LULC maps created by analyzing the Landsat TM/ETM+/OLI dataset for the years 1990, 2000, 2010, and 2020 served as the basis for change analysis. Table 2 depicts the changes in land cover categories during this period in Muzaffarpur district. The analysis of Landsat spatiotemporal data for these years revealed that the Built-Up area in the district has increased significantly. In 1990, 3.08% of the total land area was built up, which increased to 4.17% in 2000, 7.79% in 2010, and 9.76% in 2020. The vegetation area, on the other hand, decreased progressively from 1990 to 2020. The total vegetation area in the region was 15.17% in 1990, which decreased to 13.37% in 2000, further decreased to 11.26% in 2010, but slightly increased to 12.56% in 2020.

The cropland in the study area increased from 31.10% in 1990 to 33.11% hectares in 2000, but slightly decreased to 28.50% in 2010 and further decreased to 25.89% in 2020. Wetlands, which included the majority of fallow lands, decreased from 3.10% in 1990 to 2.50% in 2000, and then further to 2.04% in 2010, but showed a slight increase to 2.08% in 2020. The waterbodies group was observed to evolve more slowly than other LULC groups, with an overall area coverage of 3.31% in 1990, which decreased to 3.14% in 2000, 3.03% in 2010, and 2.57% in 2020.

Litchi, the dominant class in the study area, was treated separately from vegetation due to its high economic importance. The area used for growing Litchi increased from 1.18% in 1990 to 1.41% in 2000, 2.57% in 2010, and 3.35% in 2020. The distribution of LULC classes in Muzaffarpur district for various years, including 1990, 2000, 2010, and 2020, is shown in Fig. 2.

**Table 2:** Change in LULC during the period of 1990 to 2020

| Class Name         | 1990      |          | 2000      |          | 2010      |          | 2020      |          |
|--------------------|-----------|----------|-----------|----------|-----------|----------|-----------|----------|
|                    | Area (ha) | Area (%) |
| Built-up area      | 1534      | 3.08     | 3722      | 4.17     | 15215     | 7.79     | 23807     | 9.76     |
| Vegetation         | 48141     | 15.17    | 29749     | 13.37    | 23046     | 11.26    | 26823     | 12.56    |
| Cropland           | 98709     | 31.10    | 136799    | 33.11    | 109475    | 28.50    | 104292    | 25.89    |
| Fallow land        | 152496    | 48.06    | 133043    | 41.14    | 152218    | 38.51    | 143913    | 35.79    |
| Wetlands           | 10151     | 3.10     | 7396      | 2.50     | 6501      | 2.04     | 6616      | 2.08     |
| Waterbody          | 4179      | 3.31     | 3958      | 3.14     | 3137      | 3.03     | 3111      | 2.57     |
| Litchi cultivation | 3759      | 1.18     | 4496      | 1.41     | 8168      | 2.57     | 10597     | 3.35     |

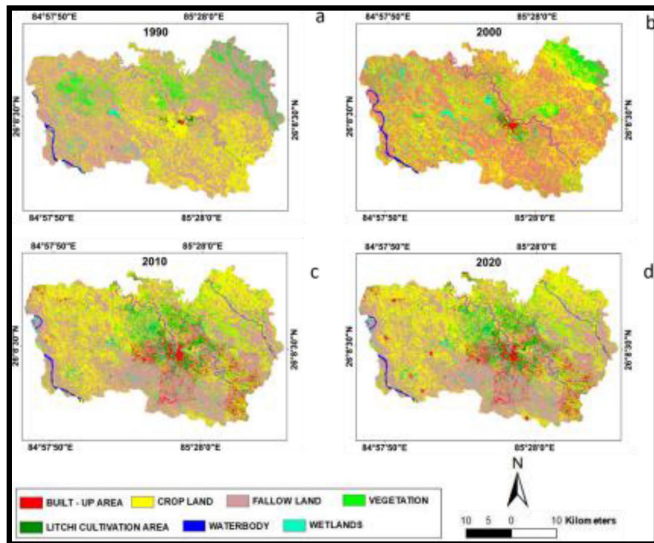


**Fig. 2:** LULC map of Muzaffarpur district, Bihar in different years

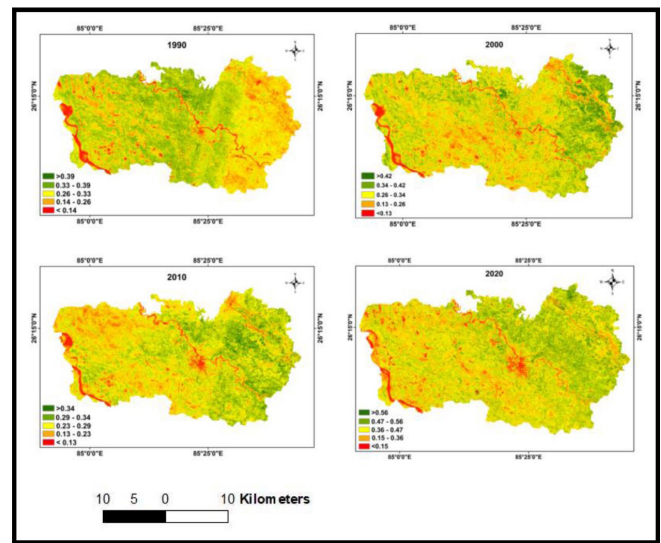


**Fig. 3:** NDVI map of Muzaffarpur district, Bihar in different years

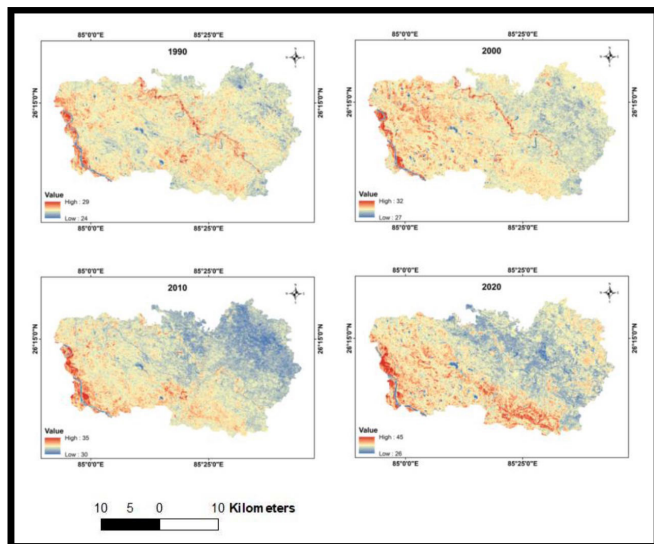


**Fig. 4:** LST map of Muzaffarpur district, Bihar in different years

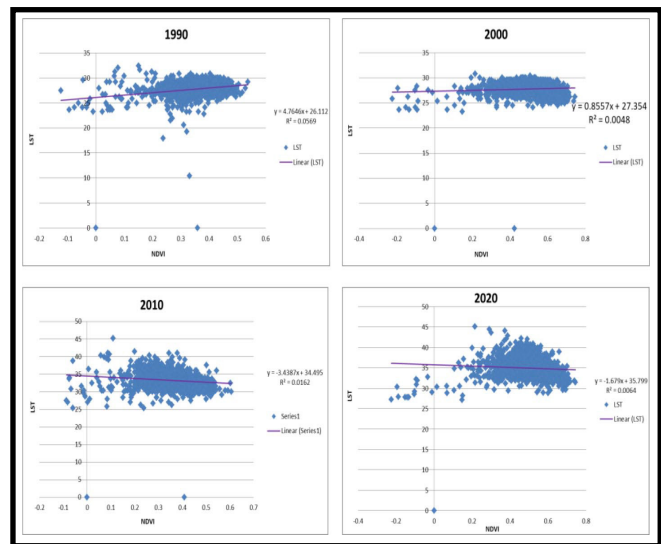


**Fig. 5:** Correlation graph between NDVI and LST

**Changes in normalized difference vegetation index (NDVI)**

In Muzaffarpur district, the spatial distribution of the Normalized Difference Vegetation Index (NDVI) is illustrated in Fig. 3. Cropland has the highest NDVI values, while urban and water areas have the lowest NDVI values. Urban areas and road networks have NDVI values between 0.1 and 0.199, and vegetation areas are

mostly concentrated in the northern part with NDVI values between 0.2 and 0.6. NDVI values around zero from -0.1 to 0.1 are primarily found in desert and barren regions, and negative values (-0.1 or less) correspond to water and wetlands. Additionally, the average NDVI values over the Muzaffarpur district gradually decreased from 1990 to 2020.

### Changes in land surface temperature (LST)

The Land Surface Temperature (LST) in Muzaffarpur district has increased gradually from 1990 to 2020, as demonstrated by Fig 4 depicting the spatial distribution of LST during the month of May for each decade during the period. Agriculture areas consistently exhibit the lowest LST, and the LST and land cover patterns are nearly identical. The central part of the district, which is predominantly covered by built-up areas, has the highest LST values. Urban areas demonstrate a higher LST in comparison to agriculture areas and water bodies, due to their high solar radiation absorption capabilities. Conversely, vegetation or water areas exhibit lower LST values due to scattering of solar radiation, plant heat absorption, and transpiration. The LST values have increased over Muzaffarpur district from 1990 to 2020 and correspond with the decline in agriculture. To mitigate the urban heat island phenomenon in Muzaffarpur district, it is essential to convert land cover to agricultural regions.

### The relationship between LST, NDVI, and land cover

The negative correlation between LST and NDVI has been extensively studied in the literature for various geographical regions (Chen *et al.*, 2006; Gorgani *et al.*, 2013; Alemu, 2019; Kumar *et al.* 2022). In all of these studies, a negative relationship between LST and NDVI was found. In Muzaffarpur District, the link between LST and NDVI was investigated using the correlation coefficient (R) and coefficient of determination ( $R^2$ ) on selected dates. Fig. 5 displays a graph demonstrating the correlation between LST and NDVI. The R values for all time periods indicate a strong negative relationship between LST and NDVI, with values exceeding 95%. Additionally,  $R^2$  values exceeding 91% indicate that changes in LST may account for more than 91% of the variation in NDVI, with less than 10% of the variation in NDVI attributed to random fluctuation. The graph in Fig. 5 illustrates that during the period trend shows lower NDVI and slightly higher LST. It was also discovered that as agricultural fields moved westward over time, LST decreased and NDVI increased in the western region. This indicates that an increase in vegetation cover results in higher NDVI and lower LST, and vice versa, where LST has a negative correlation with NDVI and vegetation cover. By examining Fig. 5, it can be observed that agriculture, urban, and water areas have a strong negative correlation with LST ( $R = -0.98$ ,  $-0.96$ , and  $-0.95$ , respectively) and a positive correlation with NDVI ( $R = 0.97$  for all three land categories).

### CONCLUSIONS

This study used remote sensing technology to investigate the temporal and spatial distribution of LST and its correlation with NDVI in the Muzaffarpur district of Bihar. The results indicated that fallow lands and sandy areas have the lowest LST and highest NDVI values, and there is a negative correlation between LST and NDVI. The findings of this study suggest the importance of preserving vegetation-based land cover in urban settings to promote biodiversity, regulate microclimates, and improve environmental health. Such preservation efforts can help to mitigate the adverse effects of land use change and promote sustainable urban development.

**Funding:** This research received no external funding.

**Data availability statement:** Data shall be available from the corresponding author on request.

**Conflict of interest statement:** The authors declare that there is no conflict of interest.

**Author Contributions:** **B. Sajan:** Methodology, software, validation, writing—original draft preparation, visualization, **S. Kanga:** Conceptualization, investigation, writing—review and editing, supervision **S. K. Singh:** Formal analysis, resources, visualization, project administration, **V. N. Mishra:** Validation, **B. Durin:** Validation, data curation. All authors have read and agreed to the published version of the manuscript.

**Disclaimer:** The contents, opinions, and views expressed in the research article published in the Journal of Agrometeorology are the views of the authors and do not necessarily reflect the views of the organizations they belong to.

**Publisher's Note:** The periodical remains neutral with regard to jurisdictional claims in published maps and institutional affiliations.

### REFERENCES

- Alemu, M. M. (2019). Analysis of Spatio-temporal Land Surface Temperature and Normalized Difference Vegetation Index Changes in the Andassa Watershed, Blue Nile Basin, Ethiopia. *J. Res. Eco.*, 10(1): 77-85. DOI:10.5814/j.issn.1674-764x.2019.01.010
- Bhagia, N, Oza, M.P., Rajak, D.R. and Dadhwal, V.K. (2005). Wheat Yield Forecast Models Using Temperature Based Simple and Weighted Indices for Punjab and Western Uttar Pradesh. *J. Agrometeorol.*, 7 (1): 115–19. DOI: <https://doi.org/10.54386/jam.v7i1.823>
- Chaudhari, K.N., Tripathy, R. and Patel, N.K. (2010). Spatial Wheat Yield Prediction Using Crop Simulation Model, GIS, Remote Sensing and Ground Observed Data. *J. Agrometeorol.*, 12 (2): 174–80. DOI: <https://doi.org/10.54386/jam.v12i2.1300>
- Chen, X. L., Zhao, H. M., Li, P. X. and Yin, Z. Y. (2006). Remote sensing image-based analysis of the relationship between. *Remote Sens. Environ.*, 104(2006), 133-146. DOI: 10.1016/j.rse.2005.11.016
- Dadhwal, V. K., and Yamini Bhat. (2023). Revisiting statistical spectral-agrometeorological wheat yield models for Punjab using MODIS EVI and NCMRWF re-analysis temperature data. *J. Agrometeorol.*, 25(1):10–17. DOI: <https://doi.org/10.54386/jam.v25i1.2067>
- Dash, P., Göttsche, F.-M., Olesen, F.-S. and Fischer, H. (2002). Land surface temperature and emissivity estimation from passive sensor data: theory and practice; current trends. *International J. Remote Sens.*, 23(13): 2563. DOI: 10.1080/01431160110115041

- Gorgani, A. S., Panahi, M., and Rezaie, F. (2013). The Relationship between NDVI and LST in the urban area of Mashhad, Iran. *International Conference on Civil Engineering Architecture & Urban Sustain. Devel.*, 1-7.
- Kumar, D.A., Neelima, T., Srikanth, P., Devi, M.U., Suresh, K. and Murthy, C. (2022). Maize yield prediction using NDVI derived from Sentinel 2 data in Siddipet district of Telangana state. *J. Agrometeorol.*, 24 (2): 165-168. DOI: <http://doi.org/10.54386/jam.v24i2.1635>
- Lambin, E., Turner, B., Geist, H. J., Agbola, S., Angelsen, A., Bruce, J., and Xu, J. (2001). The causes of land-use and land-cover change: moving beyond the myths. *Global Environ. Change*, 11: 261-269.
- Lin, B. B., Philpott, S. M., and Jha, S. (2015). The future of urban agriculture and biodiversity-ecosystem services: Challenges and next steps. *Gfo Ecol. Soc. Germany, Austria and Switzerland*, 16(3): 189-201.
- Masek, J.G., Vermote, E.F., Saleous, N., Wolfe, R., Hall, F.G., Huemmrich, F., Gao, F., Kutler, J. and Lim, T.K. (2017). LEDAPS Landsat Calibration, Reflectance, Atmospheric Correction Preprocessing Code. Orn. Dac. NASA, 2. DOI: <http://dx.doi.org/10.3334/ORNLDAAC/1146>
- Rakib, A. A., Akter, S. K., Rahman, M. N., Arpi, S. and Kafy, A. A. (2020). Analyzing the Pattern of Land Use Land Cover Change and its Impact on Land Surface Temperature: A Remote Sensing Approach in Mymensingh, Bangladesh. (B. University of Dhaka, Ed.) *Dhaka University Research Society*, 1-10.
- Richards, D. R. and Belcher, R. N. (2019). Global Changes in Urban Vegetation Cover. *Remote Sens.*, 12(1): 23. DOI: <https://doi.org/10.3390/rs12010023>
- Zhu, Z. and Curtis E. W. (2012). Object-based cloud and cloud shadow detection in Landsat imagery. *Remote Sens. Environ.*, 118:83-94. DOI: <https://doi.org/10.1016/j.rse.2011.10.028>
- Zhu, Z., Wang S. and Curtis, W. E. (2015). Improvement and expansion of the Fmask algorithm: Cloud, cloud shadow, and snow detection for Landsats 4-7, 8, and Sentinel 2 images. *Remote Sens. Environ.*, 159: 269-277. DOI: <https://doi.org/10.1016/j.rse.2014.12.014>